# Isotope Effects Reveal That *Para*-Substituted Benzylamines Are Poor Reactivity Probes of the Quinoprotein Mechanism for Aromatic Amine Dehydrogenase[†,‡]

Parvinder Hothi,[§] Anna Roujeinikova,[§] Khalid Abu Khadra,[§] Michael Lee,[||] Paul Cullis,[||] David Leys,[§] and Nigel S. Scrutton*[,§]

*Manchester Interdisciplinary Biocentre, Faculty of Life Sciences, University of Manchester, 131 Princess Street, Manchester M1 7ND, U.K., and Department of Chemistry, University of Leicester, University Road, Leicester LE1 7RH, U.K.*

*Received April 17, 2007; Revised Manuscript Received June 5, 2007*

ABSTRACT: Structure−activity correlations have been employed previously in the mechanistic interpretation of TTQ-dependent amine dehydrogenases using a series of *para*-substituted benzylamines. However, by combining the use of kinetic isotope effects (KIEs) and crystallographic analysis, in conjunction with structure−reactivity correlation studies, we show that *para*-substituted benzylamines are poor reactivity probes for TTQ-dependent aromatic amine dehydrogenase (AADH). Stopped-flow kinetic studies of the reductive half-reaction, with *para*-substituted benzylamines and their dideuterated counterparts, demonstrate that C−H or C−D bond breakage is not fully rate limiting (KIEs ∼ unity). Contrary to previous reports, Hammett plots exhibit a poor correlation of structure−reactivity data with electronic substituent effects for *para*-substituted benzylamines and phenylethylamines. Crystallographic studies of enzyme−substrate complexes reveal that the observed structure−reactivity correlations are not attributed to distinct binding modes for *para*-substituted benzylamines in the active site, although two binding sites for *p*-nitrobenzylamine are identified. We identify structural rearrangements, prior to the H-transfer step, which are likely to limit the rate of TTQ reduction by benzylamines. This work emphasizes (i) the need for caution when applying structure−activity correlations to enzyme-catalyzed reactions and (ii) the added benefit of using both isotope effects and structural analysis, in conjunction with structure−reactivity relationships, to study chemical steps in enzyme reaction cycles.

Quantitative structure−activity relationships are useful tools for probing enzyme mechanism, and *para*-substituted benzylamines have been used as reactivity probes with quinoprotein enzymes, including the tryptophan tryptophylquinone-dependent enzyme methylamine dehydrogenase (MADH)[1] (*1*) and aromatic amine dehydrogenase (AADH) (*2*). AADH catalyzes the oxidative deamination of a wide range of amines to their corresponding aldehydes and ammonia (*3*).

$$RCH_2NH_2 + H_2O = RCHO + NH_3 + 2e^- + 2H^+$$

The enzyme has an $\alpha_2\beta_2$ structure ($\alpha$, 40 kDa; TTQ-containing $\beta$, 14 kDa) and is highly similar in fold to the related TTQ-dependent methylamine dehydrogenase (MADH), which oxidizes methylamine to formaldehyde in many Gram-negative bacteria (*4*). AADH and MADH are believed to share a common mechanism for the reductive half-reaction (*1*, *2*, *5*) during which cleavage of the substrate C−H bond occurs by environmentally coupled tunneling (*6*−*8*). In the reductive half-reaction, both enzymes reduce the TTQ cofactor through the formation of a carbinolamine intermediate followed by dehydration to yield an iminoquinone (*1*). The iminoquinone decays, by breakage of the substrate C−H bond, and generates the product Schiff base. It has been proposed that an active site base abstracts a proton from the methyl carbon of the substrate, forming a carbanionic species concomitant with TTQ reduction (*1*, *2*, *5*). The oxidation of substrate by AADH and MADH proceeds via a pathway that involves the release of two electrons, which are transferred to the type I blue copper proteins azurin (AADH) and amicyanin (MADH), respectively.

AADH-catalyzed proton transfer from the substrate tryptamine to the active site base (Asp128$\beta$) occurs by quantum mechanical tunneling and is assisted by short-range

[†] The work was funded by the UK Biotechnology and Biological Sciences Research Council. N.S.S. is a BBSRC Professorial Research Fellow.

[‡] Atomic coordinates and structure factors (entries 2HJ4, 2HJB, and 2Q7Q) have been deposited in the Protein Data Bank, Research Collaboratory for Structural Bioinformatics, Rutgers University, New Brunswick, NJ.

* To whom correspondence should be addressed. E-mail: nigel.scrutton@manchester.ac.uk. Telephone: +44 161 306 5152. Fax: +44 161 306 8918.

[§] University of Manchester.

[||] University of Leicester.

[1] Abbreviations: AADH, aromatic amine dehydrogenase; BisTris, bis(2-hydroxyethyl)iminotris(hydroxymethyl)methane; DCPIP, dichlorophenolindophenol; KIE, kinetic isotope effect; LTQ, lysine tyrosylquinone; MADH, methylamine dehydrogenase; PES, phenazine ethosulfate; QSARs, quantitative structure−activity relationships; TPQ, 6-hydroxydopaquinone; TTQ, tryptophan tryptophylquinone; $CH_2Cl_2$, dichloromethane; $NaBD_4$, sodium borodeuteride; $Na_2SO_4$, anhydrous sodium sulfate; TFA, trifluoroacetic acid; THF, tetrahydrofuran; $\sigma_p$, electronic parameter for substituents in the *para* position; *F*, field/inductive parameter; *R*, resonance parameter; $\pi$, hydrophobicity parameter; $E_s$, steric parameter.

10.1021/bi7007239 CCC: $37.00 
Published on Web 07/18/2007

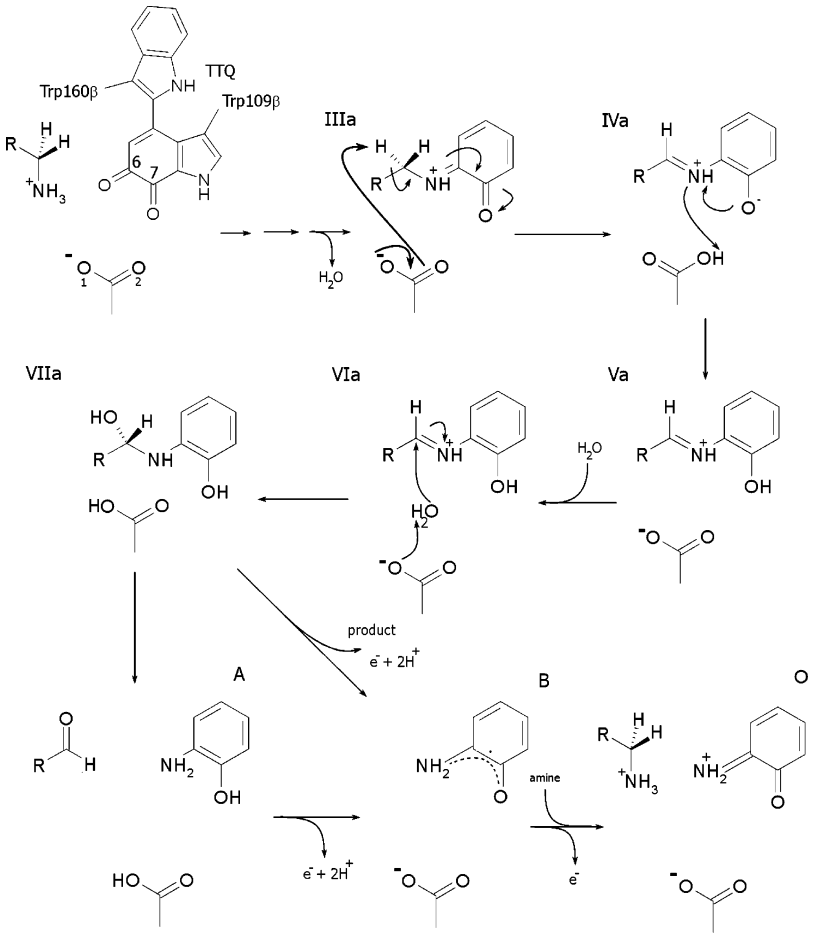


FIGURE 1: Proposed reaction scheme for the reductive half-reaction of AADH with tryptamine as the substrate based on crystallographic analysis of reaction intermediates (*8*). Intermediates are numbered with Roman numerals; for clarity, only key atoms are represented from intermediate II onward, whereas TTQ atoms C6 and C7 and Asp128$\beta$ atoms O1 and O2 are labeled for intermediate I.

motion that modulates the proton−acceptor distance (*8*, *9*). A description of the reductive half-reaction with tryptamine substrate has been reported at atomic resolution using X-ray crystallography and by using kinetic and computational methods (*8*, *10*) (Figure 1). In the oxidative half-reaction, hydrolysis of a product Schiff base produces the aminoquinol intermediate, which is converted back to the oxidized enzyme by the transfer of an electron to the physiological electron acceptor azurin (*11*). Structural reorganization of the substrate-reduced small subunit of AADH places a water/ammonia molecule, derived from the initial iminoquinone formation, within hydrogen bonding distance of O7 of TTQ where it can act as a proton acceptor during electron transfer to azurin (*12*, *13*). This proton transfer from O7 of TTQ to water is thought to be the mechanistic origin of the slower electron transfer to azurin when AADH is in the *N*-quinol, as opposed to the hydroquinone, form (*11*, *12*).

Quantitative structure−activity relationships (QSARs) are useful tools for mechanistic interpretation and have been used to probe the nature of chemical intermediates in quinoprotein enzymes (*1*, *2*, *14*, *15*). In QSAR studies, the Hammett methodology is employed to derive correlations between substituent constants and kinetic parameters (*16*). Substituent properties commonly used to probe mechanism are electronic ($\sigma_p$) [composed of both field/inductive effects (*F*) and resonance effects (*R*)], hydrophobic ($\pi$), and steric ($E_s$) (*16*). The constant *R* describes the ability of a substituent to withdraw electrons from, or release electrons into, the conjugated system of $\pi$-electrons. *F* describes the ability of a substituent to influence a process via electrostatic interactions through space (field) and intervening $\sigma$-bonds by polarization (inductive). Unlike the resonance effect, the field/inductive effect is attenuated with distance (*2*, *16*).

Derivatives of benzylamine, with substituents in the *para* position of the aromatic ring, are routinely employed in QSAR analyses of quinoprotein enzymes because of their efficiency as substrates and differing degrees of electronegativity. Structure−reactivity correlations have been reported for reactions of eukaryotic topa quinone (TPQ)-dependent bovine serum amine oxidase (*15*) and lysine tyrosylquinone (LTQ)-dependent lysyl oxidase (*14*). Observed correlations were thought to be consistent with proton abstraction and the formation of a carbanionic intermediate during the reductive half-reaction (*14*, *15*). QSAR studies with MADH have been used to probe the mechanism of TTQ reduction (imine formation) and TTQ inactivation (hydrazone formation) using *para*-substituted benzylamines and phenylhydrazines as substrates and inhibitors, respectively (*1*, *17*). A positive correlation between field/inductive effects and the limiting rate constant for TTQ reduction was attributed to the formation of a carbanionic species (*1*), and the rate of TTQ inactivation was primarily dependent on resonance, rather than field/inductive, effects (*17*). Similar correlations, between field/inductive effects and the limiting rate constant for TTQ reduction, have been reported for reactions of AADH with *para*-substituted benzylamines and phenylethy-

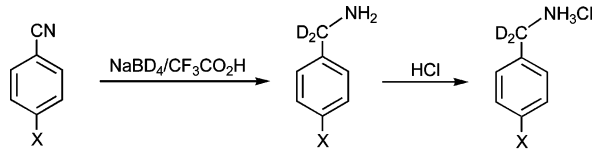


FIGURE 2: Scheme for the synthesis of dideuterated *para*-substituted benzylamines.

lamines (*2*). Thus far, structure−activity relationships have demonstrated that the reductive half-reactions of eukaryotic amine oxidases (*14*, *15*) are similar in their mechanisms, of formation of the enzyme−substrate complex and stabilization of a carbanionic intermediate, to those of bacterial amine dehydrogenases (*1*, *2*).

Herein, we have extended kinetic and QSAR studies of AADH to include an extensive series of *para*-substituted phenylethylamines, benzylamines and the dideuterated counterparts of *para*-substituted benzylamines, and by incorporating crystallographic studies. We demonstrate that the reactivity correlations are inconsistent with previously published structure−reactivity studies. Moreover, we show that *para*-substituted benzylamines are poor probes for structure−reactivity studies with AADH because the C−H or C−D bond breakage step is only partially rate limiting in the reductive half-reaction. We develop a model for the reaction of AADH based on structural analysis of enzyme−substrate complexes. This model invokes major structural reorganization in the active site prior to C−H bond breakage, a feature of the mechanism that partially limits the rate of TTQ cofactor reduction by *para*-substituted benzylamine substrates.

## EXPERIMENTAL PROCEDURES

*Materials.* BisTris propane buffer, DCPIP (2,6-dichlorophenolindophenol, sodium salt), PES (phenazine ethosulfate; *N*-ethyldibenzopyrazine ethyl sulfate salt), $\beta$-phenylethylamine, hydroxyphenylethylamine, nitrophenylethylamine, benzylamine, and *para*-substituted benzylamines were obtained from Sigma. Amino-, methyl-, fluoro-, and chlorophenylethylamines were from Acros Organics. Bromophenylethylamine was obtained from Fluorochem and methoxyphenylethylamine from Apollo Scientific Ltd. Deuterated benzylamine HCl ($C_6D_5CD_2NH_2$ HCl, 99.6%) was from CDN Isotopes. Sodium borodeuteride (99% enriched) was obtained from Cambridge Isotope Laboratories. Deuterium oxide was from Goss Scientific Instruments Ltd. The chemical purity of the deuterated reagents was determined to be >99% by high-performance liquid chromatography, NMR, and gas chromatography, by the supplier.

*Synthesis of Dideuterated Para-Substituted Benzylamines.* Dideuterated benzylamines were synthesized as shown in Figure 2 using a modification of the method reported by Umino et al. (*18*). $NaBD_4$ (15 mmol) was suspended in dry THF (10 mL), and TFA (15 mmol) in dry THF (5 mL) was added over 10 min at room temperature. The nitrile derivative (12.5 mmol) (each listed below) in dry THF (5 mL) was added to the mixture and the mixture stirred overnight. The reaction was quenched by the addition of $D_2O$ (2 mL); water was added (~20 mL), and the THF was removed by rotary evaporation. The aqueous suspension was extracted with $CH_2Cl_2$, and the combined organic extracts were dried over solid $Na_2SO_4$ and filtered to give a solution of the free benzylamine in $CH_2Cl_2$. Addition of HCl-saturated $CH_2Cl_2$ to this solution precipitated the hydrochloride salt of the corresponding amine. Yields were typically 40−50%. Benzylamine HCl salts were >95% chemically pure and 90−99% isotopically enriched, as judged from the $^1$H high-field NMR spectrum and integration of the residual N-CHD signal, respectively. $^1$H NMR spectra were recorded on a Bruker DPX NMR spectrometer. Mass spectra were recorded on a Micromass Quattro liquid chromatography−mass spectrometry system operating in electrospray mode, and accurate mass positive ion FAB spectra were recorded on a Kratos Concept spectrometer.

*Benzylamine HCl salt from reduction of benzonitrile*: $^1$H NMR ($CD_3OD$) $\delta$ 7.44 (m, 5H) [8% H-C-D @ 4.09 (s)]; MS M − H (+2HCl) 180, 2M − H (+3HCl) 325, 3M − H (+4HCl) 470, 4M − H (+5HCl) 615. Accurate mass positive ion FAB for $^{12}C_7H_8D_2N$ is expected to be 110.09382 and was determined to be 110.09388.

*4-Methylbenzylamine HCl salt*: $^1$H NMR ($D_2O$) $\delta$ 7.21−7.32 (m, 4H), 2.27 (s, 3H) [3% H-C-D @ 4.05 (br s)]; MS M − H (+2HCl) 194, 2M − H (+3HCl) 353, 3M − H (+4HCl) 512. Accurate mass positive ion FAB for $^{12}C_8H_{10}D_2N$ is expected to be 124.10950 and was determined to be 124.10953.

*4-Nitrobenzylamine HCl salt*: $^1$H NMR ($CD_3OD$) $\delta$ 8.31 (d, 2H), 7.74 (d, 2H) [7% H-C-D @ 4.27 (br s)]; MS M + 2HCl 226, 2M + 3HCl 416, 3M + 4HCl 606. Accurate mass positive ion FAB for $^{12}C_7H_7D_2N_2O_2$ is expected to be 155.07888 and was determined to be 155.07896.

*4-Methoxybenzylamine HCl salt*: $^1$H NMR ($CD_3OD$) $\delta$ 7.39 (d, 2H), 6.97 (d, 2H), 3.81 (s, 3H) [8% H-C-D @ 4.54 (br s)]; MS M − H (+2HCl) 210, 2M − H (+3HCl) 385, 3M − H (+4HCl) 560. Accurate mass positive ion FAB for $^{12}C_8H_{10}D_2NO$ is expected to be 140.10447 and was determined to be 140.10444.

*4-Fluorobenzylamine HCl salt*: $^1$H NMR ($CD_3OD$) $\delta$ 7.49 (m, 2H), 7.16 (m, 2H) [<1% H-C-D @ 4.08 (br s)]; MS M − H (+2HCl) 198, 2M − H (+3HCl) 361, 3M − H (+4HCl) 524. Accurate mass positive ion FAB for $^{12}C_7H_7D_2FN$ is expected to be 128.08445 and was determined to be 128.08446.

*4-Chlorobenzylamine HCl salt*: $^1$H NMR ($CD_3OD$) $\delta$ 7.45 (s, 4H) [<1% H-C-D @ 4.08 (br s)]; MS M − $NH_2$ 127. Accurate mass positive ion FAB for $^{12}C_7H_7{}^{35}ClD_2N$ is expected to be 144.05495 and was determined to be 144.05491.

*4-Bromobenzylamine HCl salt*: $^1$H NMR ($CD_3OD$) $\delta$ 7.60 (d, 2H), 7.40 (d, 2H) [10% H-C-D @ 4.08 (br s)]; MS M − H (+2HCl) 258, 2M − H (+3HCl) 481. Accurate mass positive ion FAB for $^{12}C_7H_7{}^{79}BrD_2N$ is expected to be 188.00436 and was determined to be 188.0439. In all cases, M is the mass of the free amine for the ES-MS, and the accurate mass positive ion FAB data are for the protonated amine cation.

*Purification of AADH. Alcaligenes faecalis* IFO 14479 was grown at 30 °C on 0.15% (w/v) $\beta$-phenylethylamine (*19*), and AADH was purified as described previously (*20*). Prior to use in kinetic studies, AADH was reoxidized with potassium ferricyanide and exchanged into 10 mM BisTris

Table 1: Kinetic Parameters Determined from Stopped-Flow Reactions of AADH with *Para*-Substituted Amines at 25 °C[a]

| | phenylethylamine | benzylamine | | | | |
|---|---|---|---|---|---|---|
| *para* substituent | $k_{lim}^{H}$ ($s^{-1}$) | $k_{lim}^{H}$ ($s^{-1}$) | $k_{lim}^{D}$ ($s^{-1}$) | $K_d^{H}$ ($\mu$M) | $K_d^{D}$ ($\mu$M) | KIE |
| H | 45.56 ± 0.3 | 1.47 ± 0.01 | 0.32 ± 0.01 | 10.38 ± 0.3 | 10.4 ± 0.3 | 4.59 ± 0.2 |
| $CH_3$ | 44.7 ± 0.3 | 0.29 ± 0.01 | 0.25 ± 0.01 | 1.93 ± 0.1 | 2.26 ± 0.1 | 1.16 ± 0.1 |
| $OCH_3$ | 417.6 ± 10.7 | 5.09 ± 0.04 | 0.94 ± 0.01 | 40.3 ± 1.7 | 14.1 ± 0.6 | 5.41 ± 0.1 |
| $NO_2$ | 29.35 ± 0.2 | 48.7 ± 0.41 | 29.8 ± 0.25 | 4.29 ± 0.2 | 4.69 ± 0.2 | 1.63 ± 0.1 |
| F | 93.13 ± 0.7 | 5.51 ± 0.04 | 0.91 ± 0.01 | 7.35 ± 0.3 | 4.77 ± 0.2 | 6.05 ± 0.1 |
| Cl | 65.5 ± 0.3 | 1.37 ± 0.01 | 0.97 ± 0.01 | <5.0 | <5.0 | 1.41 ± 0.1 |
| Br | 73.8 ± 0.3 | 1.40 ± 0.02 | 0.94 ± 0.01 | <5.0 | <5.0 | 1.49 ± 0.1 |
| OH | 412.7 ± 7.0 | – | – | – | – | – |
| $NH_2$ | 31.6 ± 0.3 | – | – | – | – | – |

[a] Fitting to the hyperbolic expression-determined $K_d$ values for *para*-substituted benzylamines as indicated, and $K_d$ (micromolar) values of 9.5 ± 0.7, 2.7 ± 0.2, and 2.5 ± 0.2 for hydroxy-, methoxy-, and aminophenylethylamines, respectively. For other *para*-substituted phenylethylamines, a lack of dependence on substrate concentration was observed ($K_d$ < 5 $\mu$M) (data not shown). For *para*-substituted amines that displayed little dependence on substrate concentration, observed rate constants measured at 200 $\mu$M ($K_d$ < 5 $\mu$M) represent the limiting rates of TTQ reduction.

Table 2: Crystallographic Data for AADH−*Para*-Substituted Benzylamine Complexes

| *para* substituent | H | $CH_3$ | $OCH_3$ | $NO_2$ | Cl |
|---|---|---|---|---|---|
| space group | $P2_1$ | $P2_1$ | $P2_12_12_1$ | $P2_1$ | $P2_12_12_1$ |
| resolution (Å) | 20−1.3 | 20−1.4 | 20−1.85 | 20−1.6 | 20−1.6 |
| average $B$ (Å$^2$) | 19.9 | 13.9 | 24.9 | 14.2 | 20.9 |
| no. of unique reflections | 224486 | 174954 | 75961 | 106519 | 127521 |
| completeness (%) | 94.7 | 99.1 | 99.0 | 96.0 | 95.2 |
| $I/\sigma I$ | 8.1 | 7.5 | 7.6 | 8.8 | 10.8 |
| $R_{cryst}/R_{free}$ | 15.8/18.6 | 13.8/17.1 | 17.6/23.1 | 16.4/20.8 | 16.7/19.3 |

propane buffer (pH 7.5) by gel exclusion chromatography. The enzyme concentration was determined using an extinction coefficient of 27 600 $M^{-1}$ $cm^{-1}$ at 433 nm (*3*).

*Stopped-Flow Kinetic Studies of the Reductive Half-Reaction*. Rapid kinetic studies of the reductive half-reaction were performed using an Applied Photophysics SX.18MV stopped-flow spectrophotometer. Oxidized AADH (reaction cell concentration of 1 $\mu$M) in 10 mM BisTris propane buffer (pH 7.5) was rapidly mixed with various concentrations of substrate (see Results), at 25 °C. TTQ reduction was followed at 456 nm. Data were analyzed by nonlinear least-squares regression analysis on an Acorn RISC PC using Spectrakinetics software (Applied Photophysics). For each substrate concentration, at least three replica measurements were collected and averaged, each containing 1000 data points. Under pseudo-first-order conditions, absorbance changes accompanying enzyme reduction were monophasic or biphasic in nature ($k_1$, >85% of the total amplitude change) and were analyzed by fitting to a standard single- or double-exponential expression, respectively. Where appropriate, the concentration dependence of $k_{obs}$ was analyzed by being fit to the standard hyperbolic expression (*21*) to obtain values for the apparent dissociation constant for the enzyme−substrate complex, $K_d$, and the limiting rate, $k_{lim}$, of TTQ reduction.

*Crystallography*. Crystals were grown as previously described (*8*). Crystals of oxidized AADH were briefly immersed in mother liquor supplemented with 10% PEG 400 and 10 mM benzylamine/substituted *p*-benzylamines until the crystals were fully discolored (demonstrating complete reduction). Data on single flash-cooled crystals were collected at ESRF beam lines (see Table 2). Diffraction data were analyzed and merged using DENZO and SCALEPACK (*22*) and the corresponding structures refined using REFMAC5 (*23*). Final data and refinement statistics are given in Table 2.

## RESULTS

*Stopped-Flow Studies of the Reductive Half-Reaction of AADH with Para-Substituted Amines*. Previous kinetic and QSAR studies with *para*-substituted benzylamines and phenylethylamines have indicated major inductive effects on C−H bond breakage in the reductive half-reaction of AADH (*2*). We have extended the range of substrates used in structure−reactivity correlations and synthesized the corresponding dideuterated *para*-substituted benzylamines to obtain information about KIEs associated with the C−H or C−D bond breakage reaction.

Dideuterated benzylamines were synthesized as described in Experimental Procedures and were 90−99% isotopically enriched, as judged from the $^1$H high-field NMR spectrum and integration of the residual N-CHD signal. We have previously demonstrated that isotopic impurities, of approximately ≤10%, have negligible effects on kinetic parameters obtained from stopped-flow studies (*24*). Therefore, rate constants and KIEs reported in this study did not require correction for isotopic impurities (<10% for dideuterated *para*-substituted benzylamines). Reduction of the TTQ cofactor was followed at 456 nm on rapid mixing of enzyme with substrate. Kinetic parameters obtained with dideuterated benzylamine ($C_6H_5CD_2NH_2$ HCl) were comparable to parameters obtained with commercially available perdeuterated benzylamine ($C_6D_5CD_2NH_2$ HCl; CDN Isotopes). On the basis of the limiting rate constant for TTQ reduction, KIEs of 4.6 ± 0.2 and 4.2 ± 0.1 were obtained with perdeuterated and dideuterated benzylamine, respectively. During steady-state reactions of AADH, KIEs of 2.5 ± 0.2 and 2.4 ± 0.2 were obtained with perdeuterated

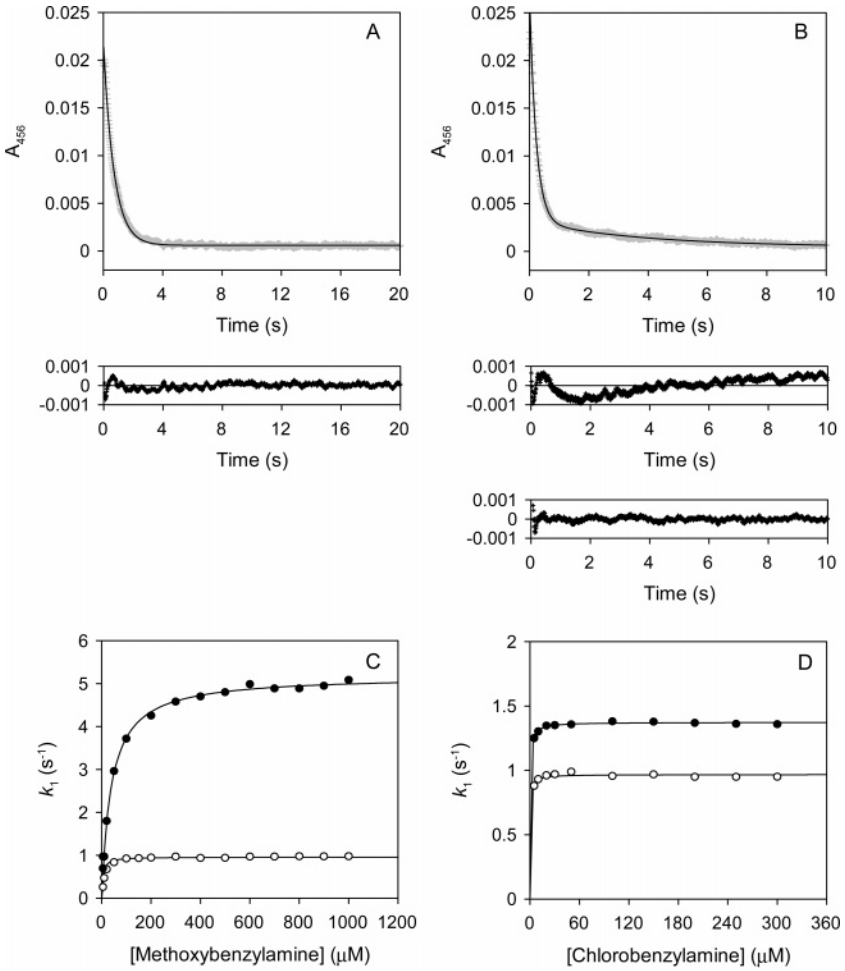


FIGURE 3: Stopped-flow kinetic data for the reaction of AADH with *para*-substituted benzylamines. (A) Example of the monophasic absorbance change monitored at 456 nm with benzylamine, methylbenzylamine, and nitrobenzylamine. Reactions were performed using 1 $\mu$M enzyme (reaction cell concentration) in 10 mM BisTris propane buffer (pH 7.5) at 25 °C. The monophasic fit to the data (black) is shown superimposed over the raw data (gray). The bottom panel shows a plot of residuals from the fit to a monophasic rate expression. (B) Example of the biphasic absorbance change monitored at 456 nm for methoxy-, fluoro-, chloro-, and bromobenzylamine-dependent reactions. The biphasic fit to the data (black) is shown superimposed over the raw data (gray). The middle panel shows a plot of residuals from the poor fit to a monophasic rate expression. The bottom panel shows a plot of residuals from the fit to a biphasic rate expression. (C) Concentration dependence of the fast phase ($k_1$) observed at 456 nm with methoxybenzylamine. Observed rates were obtained by fitting to a double-exponential expression [concentration dependence of the slow phase ($k_2$) shown in Figure S1]. The fits shown are to the standard hyperbolic expression: (●) protiated methoxybenzylamine and (○) dideuterated methoxybenzylamine. (D) Same as panel C but for chlorobenzylamine. Similar plots were obtained with other *para*-substituted benzylamines and phenylethylamines (data not shown).

and dideuterated benzylamine, respectively (data not shown). In stopped-flow studies, absorbance changes accompanying enzyme reduction were monophasic [for *para*-substituted phenylethylamines, benzylamine, and methyl- and nitrobenzylamines (Figure 3A)] or biphasic [methoxy-, fluoro-, chloro-, and bromobenzylamines (Figure 3B)].[2]

Variation in the limiting rate constant for TTQ reduction was observed across both reactivity series (Table 1). Accurate $K_d$ values were obtained for *para*-substituted amines that displayed a hyperbolic dependence on substrate concentration under pseudo-first-order conditions (Figure 3C and Table 1). For *para*-substituted amines that demonstrated a lack of dependence on substrate concentration (Figure 3D), it was assumed that $K_d$ values were $<5$ $\mu$M (Table 1). With the exception of protiated methoxybenzylamine ($40 \pm 1.7$ $\mu$M),[3] protiated and dideuterated benzylamines had similar $K_d$ values [$<14$ $\mu$M (Table 1)]. KIEs close to unity were observed for reactions of AADH with methylbenzylamines ($1.16 \pm 0.1$), chlorobenzylamines ($1.4 \pm 0.1$), bromobenzylamines ($1.5 \pm 0.1$) and nitrobenzylamines ($1.6 \pm 0.1$), suggesting that C−H or C−D bond breakage is not fully rate limiting in the reductive half-reaction with these substrates.[4] Larger KIEs were observed for methoxybenzylamines ($5.4 \pm 0.1$) and fluorobenzylamines ($6.0 \pm 0.1$) [similar to the KIE observed with unsubstituted benzylamine ($4.6 \pm 0.2$)]. Plots of the observed rate constant versus methoxybenzylamine (KIE $= 5.4 \pm 0.1$) and chlorobenzy-

[2] Contrary to previous reports (*2*), *para*-substituted benzylamines are substrates (albeit poor) during steady-state reactions of AADH. Moreover, turnover numbers for the rate-limiting step are comparable to those of slow reactions ($k_{obs2}$) observed during stopped-flow studies of the reductive half-reaction (see Table S1 and Figure S1 of the Supporting Information).

[3] The origin of the larger $K_d$ observed for protiated methoxybenzylamine is unclear but consistent with published kinetic parameters for the reactions of *para*-substituted benzylamines with AADH (*2*).

[4] Kinetic studies of the reductive half-reaction of AADH with dideuterated *para*-substituted phenylethylamines (P. Hothi, D. Leys, and N. S. Scrutton, unpublished data) and dopamine (*7*) have demonstrated inflated KIEs of ~15.

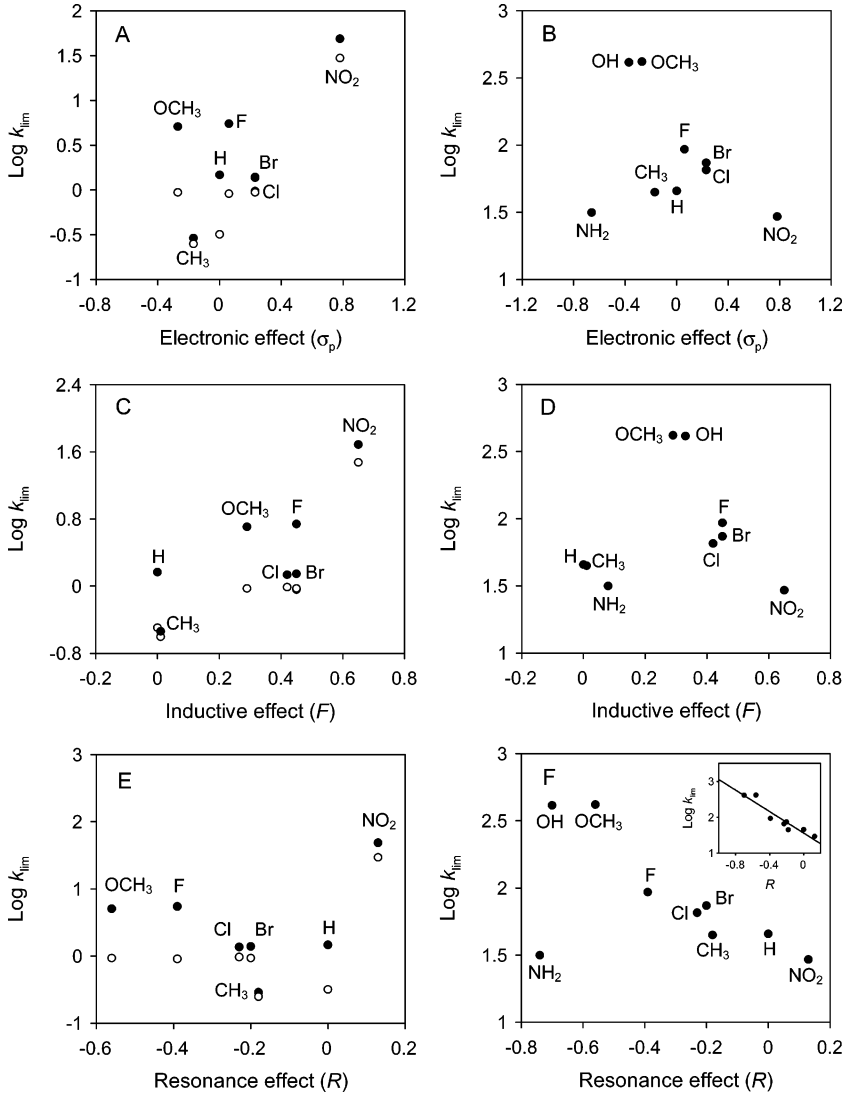


FIGURE 4: Hammett plots for structure−reactivity correlations in AADH. (A) Plot of log $k_{lim}$ vs electronic effects ($\sigma_p$) for the reactions of AADH with *para*-substituted benzylamines. Reactions were performed as described in the legend of Figure 3: (●) protiated *para*-substituted benzylamines and (○) dideuterated *para*-substituted benzylamines. For clarity, only the protiated substrates (●) are labeled. (B) Same as panel A but for the reactions of AADH with *para*-substituted phenylethylamines. (C and D) Hammett plots of log $k_{lim}$ vs field/inductive effects (*F*) for *para*-substituted benzylamines and phenylethylamines, respectively. (E) Hammett plot of log $k_{lim}$ vs resonance effects (*R*) for *para*-substituted benzylamines. (F) Same as panel E but for *para*-substituted phenylethylamines. The inset shows the linear regression of data presented in the main panel (slope, $-1.5 \pm 0.2$; without aminophenylethylamine which deviates from linear behavior).

lamine (KIE = $1.4 \pm 0.1$) concentration are shown in panels C and D of Figure 3, respectively.

*Structure−Reactivity Correlations*. Previous structure−reactivity studies with AADH have reported correlations between reactivity and field/inductive effects. Rate constants for TTQ reduction were reported to correlate linearly with the increasing electronegativity of *para* substituents, supporting the involvement of a carbanionic intermediate during the reductive half-reaction (*2*). Herein, we report structure−reactivity studies with an extended series of *para*-substituted phenylethylamines, *para*-substituted benzylamines, and their dideuterated counterparts. To probe the influence of electronic properties on TTQ reduction, AADH activity was correlated with electronic ($\sigma_p$), field/inductive (*F*), and resonance (*R*) effects. Substituent constants were obtained from Hansch and Leo (*25*) and Hansch et al. (*16*) The *R* and *F* constants are modified Swain−Lupton constants that have been adjusted to the same scale as the Hammett constants. Reactions were performed as described in Stopped-Flow Studies of the Reductive Half-Reaction, and Hammett plots were constructed by plotting the logarithm of the limiting value for TTQ reduction (Table 1) versus $\sigma_p$, *F*, and *R* parameters. An increase in electronegativity is represented by negative to positive values on Hammett plots.

We observed a poor correlation of the structure−reactivity data with electronic substituent effects (Figure 4). With *para*-substituted benzylamines, the most electron-withdrawing group (nitro) activates bond cleavage ~30-fold (Table 1), and the opposite scenario occurs with the *para* substituent (methyl) that donates electrons to the cleavable bond. However, this correlation does not extend to all *para*-substituted benzylamines. The halogen substituents have similar *F* constants (*16*); thus, for strong correlations between field/inductive effects and TTQ reduction, similar $k_{lim}$ values are expected with these substrates. On the other hand, rate constants are reduced for chloro- and bromobenzylamines (~1.4 $s^{-1}$ compared to ~5.5 $s^{-1}$ for fluorobenzylamine), and deviation from linear behavior is observed in Hammett plots

(Figure 4A,C). In previously published structure−reactivity studies (*2*), chloro- and bromobenzylamines have been omitted from the Hammett plot of log $k_{lim}$ versus $F$. Moreover, we demonstrate that *para*-substituted benzylamines are poor probes for structure−reactivity studies with AADH because of the kinetic complexity in the reductive half-reaction [KIEs close to unity (Table 1)]; i.e., the chemical step is not fully rate limiting. The KIEs obtained contrast markedly with those measured for other substrates such as tryptamine (55 ± 6) (*7*, *8*), dopamine (12.9 ± 0.2) (*7*), and phenylethylamine (15.3 ± 0.2) (P. Hothi, D. Leys, and N. S. Scrutton, unpublished data).

The breakdown in structure−reactivity correlations is more pronounced with *para*-substituted phenylethylamines (Figure 4B,D). Previous studies with these amines have reported a weak (but linear) correlation between the rate of TTQ reduction and $F$, and this was attributed to field/inductive effects being attenuated with distance (*2*). With an extended series of *para*-substituted phenylethylamines, in which substituents with strong electron withdrawing/donating properties are included, we observe no correlation between log $k_{lim}$ and $F$ (Figure 4D). Poor structure−reactivity correlations, together with the observed KIEs for *para*-substituted benzylamines, emphasize the limitations of using structure−reactivity correlations as probes of mechanism for complex enzyme reactions.

No significant correlation was observed for log $k_{lim}$ versus $R$ for *para*-substituted benzylamines (Figure 4E). If the amino group is excluded, a negative slope (−1.5 ± 0.2) was observed for the phenylethylamines, suggesting that increasing resonance effects decrease the rate of TTQ reduction (Figure 4F). Structure−reactivity correlations in enzyme-catalyzed reactions could be complicated by hydrophobic and steric interactions between ring substituents and active site residues (*25*). These parameters were investigated here, and no correlations were observed between log $k_{lim}$ and hydrophobic ($\pi$) or steric ($E_s$) effects[5] for both series of *para*-substituted amines. Furthermore, no significant correlations were observed between KIEs and $\sigma_p$, $F$, $R$, $\pi$, and $E_s$ constants. Substituent effects on $K_d$ were explored by plotting the logarithm of $K_d$ for benzylamines (Table 1) against $\sigma_p$, $F$, $R$, $\pi$, and $E_s$ constants. Insignificant correlations were observed in all cases.

*Crystal Structures of AADH−Para-Substituted Benzylamine Complexes*. To establish that observed structure−reactivity correlations were not attributed, in part, to the presence of distinct binding modes (and to investigate reaction intermediates prior to H-tunneling; see the following section), the structures of several *para*-substituted benzylamine−reduced AADH complexes were determined. These were compared with those of the corresponding tryptamine−AADH complex and oxidized AADH [which is structurally similar to the tryptamine-bound complex (*8*)]. The enzyme−substrate complex obtained with conventional benzylamine (Figures 5A and 6) is highly similar to our recently determined structures with tryptamine (*8*). The substrate amine group is placed within hydrogen bonding distance of the backbone oxygen of residues $\beta$84, $\beta$156, and $\beta$158. Furthermore, it is in close contact with a water molecule bound to the catalytic Asp$\beta$128. These observations support binding of the protonated substrate, and our proposed mechanism for initial substrate deprotonation by Asp$\beta$128 acting via the observed water molecule (see Figure 1). The crystal structures for methyl-, methoxy-, and chlorobenzylamine−enzyme complexes are highly similar to that of the benzylamine complex (Figure 5). In each case, the *para* group is in close contact with the side chains Leu$\alpha$100 and Asn$\alpha$124 and the Gly$\alpha$178 backbone.

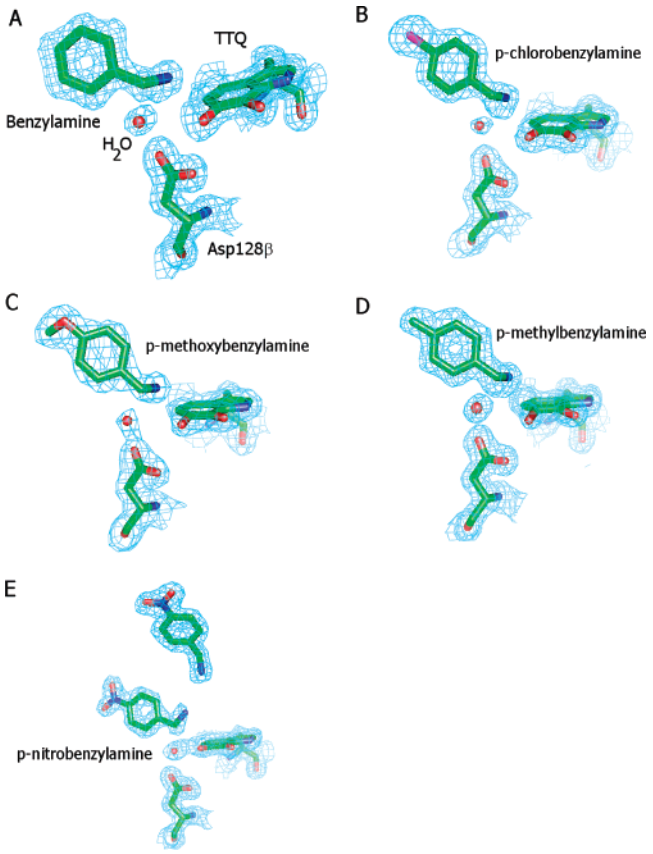


FIGURE 5: Position of various *para*-substituted benzylamines in the AADH active site. For clarity, only the active side acid−base Asp128$\beta$ and the TTQ Trp109$\beta$ derived atoms in addition to the water molecule bound between Asp128$\beta$ and the substrate amine function are shown. The $\sigma$A-weighted $2F_o - F_c$ electron density is contoured at 1.5$\sigma$ and depicted in blue.

In the nitrobenzylamine−enzyme complex, the substrate adopts a very similar conformation as described for the other *para*-substituted benzylamines, but the amine group is pointing away from the TTQ cofactor (Figure 7). This change in conformation is likely attributed to the binding of a second substrate molecule close to the active site. The latter affects the conformation of Asp$\beta$84 which in turn is likely to influence the exact position of the substrate amine group. Nevertheless, the nitrobenzylamine−enzyme complex reveals that the substrate occupies a similar position in the active site.

*Structural Rearrangement (partly) Limits Reaction with Benzylamines*. In contrast to phenylethylamine and tryptamine substrates, the aromatic moiety of the benzylamine substrates is directly attached to the carbon undergoing enzyme-catalyzed oxidation. Although the initial binding mode of both substrate categories is similar, the corresponding

[5] Several steric parameters have been described in the literature (*26*−*28*). The $E_s$ constants used here were determined from van der Waals radii of substituents. Nitrobenzylamine was not included because significantly different $E_s$ values exist for this substituent (*27*).

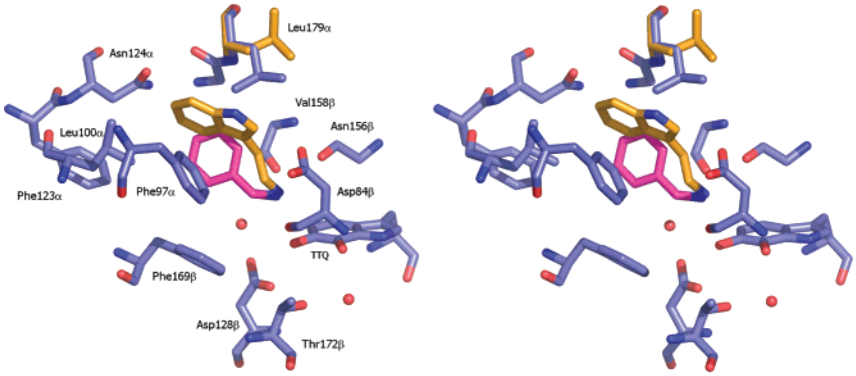


FIGURE 6: Stereoview of the benzylamine−AADH active site complex. Active site residues are depicted with atom-colored sticks with the benzylamine substrate in magenta carbons (protein carbons colored light blue). For comparison, a tryptamine molecule from the tryptamine−AADH complex (*8*) is depicted with brown carbons, as well as Leu179α, a residue that changes position upon tryptamine binding.

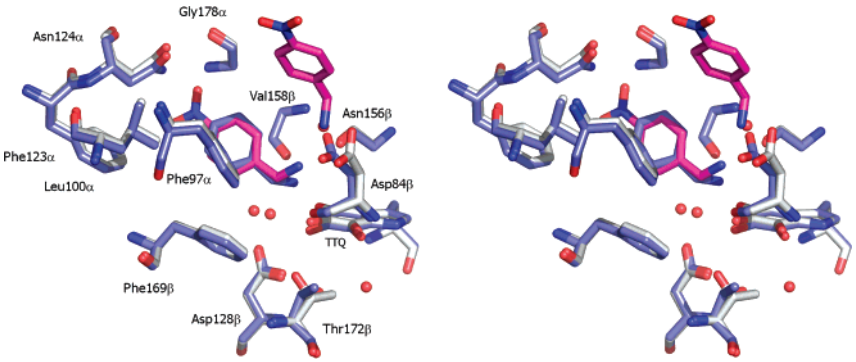


FIGURE 7: Stereoview of the *p*-nitrobenzylamine−AADH active site complex. Active site residues are depicted with atom-colored sticks with the *p*-nitrobenzylamine substrate in magenta carbons (protein carbons colored light blue). For comparison, the benzylamine−AADH complex is superimposed and depicted with gray carbons.

iminoquinone intermediates are likely to be significantly different. The modeled tryptamine iminoquinone complex (*8*), and the crystal structure of a phenylethanolamine-derived iminoquinone complex (*13*), reveal that the aromatic moiety occupies a position in the active site very similar to that observed for the respective enzyme−substrate complexes. Thus, the motions of the key N1, C1, and C2 atoms during catalysis do not significantly affect the aromatic moiety position. With the benzylamines, however, the C2 atom is part of the aromatic moiety itself, and thus, large reorganization of the benzyl side chain must occur during catalysis. For the benzylamine-derived iminoquinone complex, the requirement for the N1, C1, and C2 atoms to be in a position approximately coplanar with the TTQ aromatic plane is likely to place the benzyl side chain stacked with Pheα169. The latter can occur only if corresponding motions occur for the side chain of Pheα97 in addition to the Aspα84 backbone (Figure 8). From our crystallographic studies, we infer that TTQ reduction with benzylamines is limited by structural reorganization prior to H-tunneling (contributing to the deflated KIEs observed in the reductive half-reaction). This is consistent with thermodynamic parameters obtained from our solution studies of AADH with benzylamine, phenylethylamine, and tryptamine (see the Discussion). The required reorganization is larger with *para*-substituted benzylamines, and additional motions (e.g., motion of Leuα100) are required to accommodate the position of the nitro substituent. In accordance with this, *para*-substituted benzylamines with KIEs close to unity have larger $\Delta H^{\ddagger}$ values (see the Discussion).

## DISCUSSION

Major limitations with regard to studying enzyme mechanism are that enzyme-catalyzed reactions are complex, many physical steps are usually involved (i.e., substrate binding, product release, and protein rearrangements), and the chemical or isotope-dependent step is not always rate-limiting. This is demonstrated herein, as our kinetic studies with *para*-substituted benzylamines reveal KIEs close to unity in the reductive half-reaction of AADH (Table 1). Contrary to previous structure−reactivity studies (in which stabilization of a carbanionic intermediate was inferred) (*2*), we have demonstrated, by combining isotope effects with QSAR and structural analyses, that *para*-substituted benzylamines are inappropriate for probing the chemical mechanism of TTQ reduction in AADH. Given the common application of QSAR analyses to probing the nature of chemical intermediates in enzyme systems (*1*, *2*, *14*, *15*), this work emphasizes (i) the need for caution when applying structure−activity correlations to enzyme-catalyzed reactions and (ii) the importance of coupling isotope effects and structural analysis to QSAR studies.

We have been able to elucidate the mechanistic origin of the KIEs reported in this study through an atomic-level description of the reaction catalyzed by AADH with benzylamine substrates. In contrast to other amine substrates, the aromatic moiety of the benzylamines is directly attached to the carbon undergoing enzyme-catalyzed oxidation, and the iminoquinone intermediate is significantly different (Figure 8) from the tryptamine (*8*)- and phenylethanolamine (*13*)-derived iminoquinone complexes. Formation of the

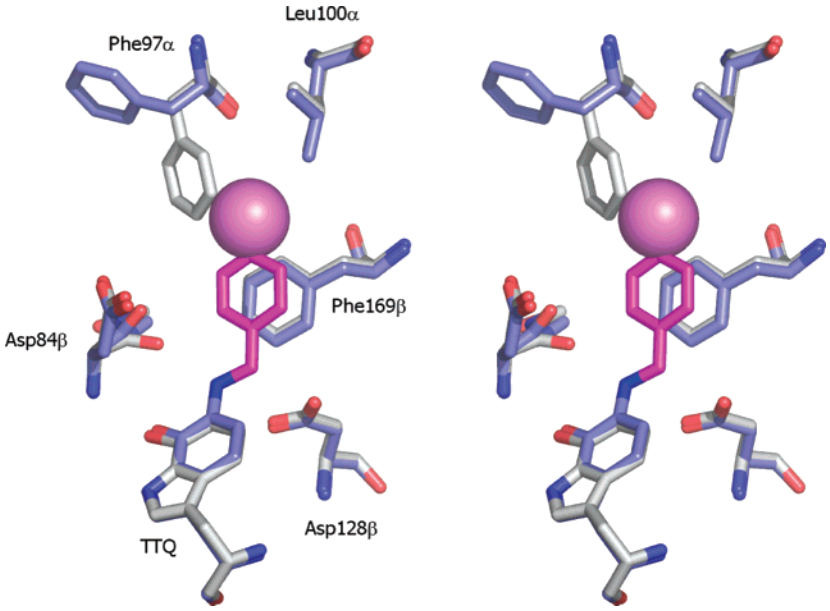


FIGURE 8: Stereoview of the proposed *para*-substituted benzylamine intermediate III structure. Active site residues are depicted with atom-colored sticks with the *para*-substituted benzylamine substrate in magenta carbons (protein carbons colored light blue). For comparison, corresponding positions of key active site amino acids in the benzylamine−AADH complex are superimposed and depicted with gray carbons. The *para* substituent is depicted as a large magenta sphere.

benzylamine-derived iminoquinone requires structural rearrangement of the benzyl side chain, which requires corresponding motions for the side chain of Pheα97 and the Aspα84 backbone (Figure 8). Clearly, larger structural reorganizations and additional motions are required to accommodate larger substituents. With this in mind, we have proposed that major structural reorganization in the active site, prior to C−H bond breakage, compromises the rate of TTQ reduction by benzylamine substrates.

The required molecular reorganization, and the limited rate of TTQ reduction for benzylamines, is consistent with thermodynamic data obtained with amine substrates studied thus far. Values of $\Delta H^{\ddagger}$ for reactions of AADH with tryptamine ($\Delta H^{\ddagger H} = 57.3 \pm 3.4$ kJ/mol, and $\Delta H^{\ddagger D} = 53.5 \pm 1.2$ kJ/mol) (*7*, *8*) are similar to those with *β*-phenylethylamine ($\Delta H^{\ddagger H} = 54.7 \pm 0.6$ kJ/mol, and $\Delta H^{\ddagger D} = 54.3 \pm 0.7$ kJ/mol) (P. Hothi, D. Leys, N. S. Scrutton, unpublished data) and significantly lower than those of benzylamine ($\Delta H^{\ddagger H} = 63.6 \pm 0.6$ kJ/mol, and $\Delta H^{\ddagger D} = 65 \pm 0.7$ kJ/mol). Moreover, larger values of $\Delta H^{\ddagger}$ are obtained for those *para*-substituted benzylamines (with the exception of nitrobenzylamine; see below) that have KIEs close to unity [∼72 ± 1 kJ/mol (Table 3)]. We have previously demonstrated that with benzylamine the KIE was measurably temperature independent (*7*). This is consistent with the enzyme−substrate complex being geometrically identical for protiated and deuterated substrates and with the protein reorganization of the enzyme−substrate complex being independent of isotope. With the tryptamine substrate, C−H bond cleavage occurs by tunneling, is fully rate limiting in the reductive half-reaction, and is accompanied by a highly inflated KIE (55) (*7*) that is measurably independent of temperature. This is clearly not the case with benzylamine substrates where we infer (partially) rate-limiting structural reorganization (that is independent of isotopic substitution) is necessary prior to bond cleavage. That the observed KIE (∼4) with benzylamine remains measurably independent of temperature (*7*) suggests H-transfer occurs by quantum mechanical tunneling.

Table 3: Kinetic and Thermodynamic Parameters Determined from Stopped-Flow Reactions of AADH with Protiated and Dideuterated *Para*-Substituted Benzylamines (investigated temperature range of 4−40 °C)[a]

| *para* substituent | $\Delta H^{\ddagger H}$ (kJ/mol) | $\Delta H^{\ddagger D}$ (kJ/mol) | KIE at 24 °C |
|---|---|---|---|
| H | 63.6 ± 0.6 | 65.0 ± 0.7 | 4.7 ± 0.1 |
| $CH_3$ | 70.3 ± 0.6 | 70.5 ± 0.6 | 1.17 ± 0.05 |
| $OCH_3$ | 66.4 ± 0.5 | 69.7 ± 0.8 | 5.03 ± 0.2 |
| $NO_2$ | 66.5 ± 1.1 | 63.9 ± 0.6 | 1.64 ± 0.1 |
| F | 62.5 ± 0.8 | 65.5 ± 1.0 | 6.08 ± 0.4 |
| Cl | 73.6 ± 0.6 | 70.7 ± 0.8 | 1.42 ± 0.1 |
| Br | 72.8 ± 0.8 | 71.3 ± 0.6 | 1.25 ± 0.1 |

[a] Parameters were obtained from fitting data to the Eyring equation as described previously (*6*). With the exception of nitrobenzylamine, *para*-substituted benzylamines with KIEs that approximate unity have greater $\Delta H^{\ddagger}$ values. It should be noted that kinetic and thermodynamic parameters obtained for nitrobenzylamine are compromised by the binding of a second substrate molecule close to the active site.

The compromised rate of TTQ reduction with benzylamine substrates is consistent with the magnitude of the observed isotope effect (4.6 compared to 13 and 55 for benzylamine, dopamine, and tryptamine, respectively) (*7*, *8*). Within the reactivity series, KIEs suggest that C−H bond breakage is more (but not fully) rate limiting for some benzylamine substrates (benzylamine, methoxybenzylamine, and fluorobenzylamine have KIEs greater than unity). Nitrobenzylamine is the "fastest" substrate within the benzylamine reactivity series, but a small KIE is observed (1.6). On the basis of kinetic studies with substrates "faster" than benzylamines (such as tryptamine and dopamine for which inflated KIEs are observed) (*7*, *8*), we would expect nitrobenzylamine to have a larger KIE [$k_{lim} \sim 48$ s$^{-1}$ compared to 5 or 1.5 s$^{-1}$ for other benzylamines (Table 1)]. Given that our crystallographic studies of the nitrobenzylamine−enzyme complex reveal that the amine group is pointing away from the TTQ cofactor (Figure 7) due to the presence of a second substrate

molecule, we believe that solution data for this substrate may be compromised and need to be rationalized with caution. Structural information gained from the nitrobenzylamine−enzyme complex herein emphasizes the importance of combining structural analysis with QSAR studies.

*Concluding Remarks*. We have shown that structure−activity correlations can be compromised in enzyme systems due to "hidden" complexities in the reaction cycle. Stable isotope and structural studies, used in conjunction with structure−reactivity studies, can provide additional and important information when probing the chemical step. Substituted amines are nonphysiological substrates used as reactivity probes with a number of enzyme systems. Suboptimal geometries of enzyme complexes with nonphysiological substrates can lead to kinetic complexity as a requirement for structural change prior to the chemical step. We suggest that the significance of rate-limiting conformational change should be assessed routinely by incorporating isotopically labeled substrates into reactivity probe studies. Structural analysis of the enzyme−substrate complex is also required in probing for alternate geometries that might have an impact on reactivity.

## SUPPORTING INFORMATION AVAILABLE

Kinetic parameters determined for steady-state and stopped-flow reactions ($k_{obs2}$) of AADH with *para*-substituted benzylamines (Table S1) and steady-state and stopped-flow kinetic data for reactions of AADH with *para*-substituted benzylamines (Figure S1). This material is available free of charge via the Internet at http://pubs.acs.org.

## REFERENCES


1. Davidson, V. L., Jones, L. H., and Graichen, M. E. (1992) Reactions of benzylamines with methylamine dehydrogenase. Evidence for a carbanionic reaction intermediate and reaction mechanism similar to eukaryotic quinoproteins, *Biochemistry 31*, 3385−3390.
2. Hyun, Y. L., and Davidson, V. L. (1995) Mechanistic studies of aromatic amine dehydrogenase, a tryptophan tryptophylquinone enzyme, *Biochemistry 34*, 816−823.
3. Govindaraj, S., Eisenstein, E., Jones, L. H., Sanders-Loehr, J., Chistoserdov, A. Y., Davidson, V. L., and Edwards, S. L. (1994) Aromatic amine dehydrogenase, a second tryptophan tryptophylquinone enzyme, *J. Bacteriol. 176*, 2922−2929.
4. Davidson, V. L. (1993) in *Principles and Applications of Quinoproteins* (Davidson, V. L., Ed.) pp 73−95, Marcel Dekker, Inc., New York.
5. Brooks, H. B., Jones, L. H., and Davidson, V. L. (1993) Deuterium kinetic isotope effect and stopped-flow kinetic studies of the quinoprotein methylamine dehydrogenase, *Biochemistry 32*, 2725−2729.
6. Basran, J., Sutcliffe, M. J., and Scrutton, N. S. (1999) Enzymatic H-transfer requires vibration-driven extreme tunneling, *Biochemistry 38*, 3218−3222.
7. Basran, J., Patel, S., Sutcliffe, M. J., and Scrutton, N. S. (2001) Importance of barrier shape in enzyme-catalyzed reactions. Vibrationally assisted hydrogen tunneling in tryptophan tryptophylquinone-dependent amine dehydrogenases, *J. Biol. Chem. 276*, 6234−6242.
8. Masgrau, L., Roujeinikova, A., Johannissen, L. O., Hothi, P., Basran, J., Ranaghan, K. E., Mulholland, A. J., Sutcliffe, M. J., Scrutton, N. S., and Leys, D. (2006) Atomic description of an enzyme reaction dominated by proton tunneling, *Science 312*, 237−241.
9. Johannissen, L. O., Hay, S., Scrutton, N. S., and Sutcliffe, M. J. (2007) Proton tunneling in aromatic amine dehydrogenase is driven by a short-range sub-picosecond promoting vibration: Consistency of simulation and theory with experiment, *J. Phys. Chem. B 111*, 2631−2638.
10. Masgrau, L., Ranaghan, K. E., Scrutton, N. S., Mulholland, A. J., and Sutcliffe, M. J. (2007) Tunneling and classical paths for proton transfer in an enzyme reaction dominated by tunneling: Oxidation of tryptamine by aromatic amine dehydrogenase, *J. Phys. Chem. B 111*, 3032−3047.
11. Hyun, Y. L., and Davidson, V. L. (1995) Electron transfer reactions between aromatic amine dehydrogenase and azurin, *Biochemistry 34*, 12249−12254.
12. Roujeinikova, A., Scrutton, N. S., and Leys, D. (2006) Atomic level insight into the oxidative half-reaction of aromatic amine dehydrogenase, *J. Biol. Chem. 281*, 40264−40272.
13. Roujeinikova, A., Hothi, P., Masgrau, L., Sutcliffe, M. J., Scrutton, N. S., and Leys, D. (2007) New insights into the reductive half-reaction mechanism of aromatic dehydrogenase revealed by reaction with carbinolamine substrates, *J. Biol. Chem.* (in press).
14. Williamson, P. R., and Kagan, H. M. (1987) Electronegativity of aromatic amines as a basis for the development of ground state inhibitors of lysyl oxidase, *J. Biol. Chem. 262*, 14520−14524.
15. Hartmann, C., and Klinman, J. P. (1991) Structure-function studies of substrate oxidation by bovine serum amine oxidase: relationship to cofactor structure and mechanism, *Biochemistry 30*, 4605−4611.
16. Hansch, C., Leo, A., and Taft, R. W. (1991) A survey of Hammett substituent constants and resonance and field parameters, *Chem. Rev. 91*, 165−195.
17. Davidson, V. L., and Jones, L. H. (1995) Reaction mechanism for the inactivation of the quinoprotein methylamine dehydrogenase by phenylhydrazine, *Biochim. Biophys. Acta 1252*, 146−150.
18. Umino, N., Iwakuma, T., and Itoh, N. (1976) Sodium acyloxyborohydride as new reducing agents. II. Reduction of nitriles to the corresponding amines, *Tetrahedron Lett*., 2875−2876.
19. Iwaki, M., Yagi, T., Horiike, K., Saeki, Y., Ushijima, T., and Nozaki, M. (1983) Crystallization and properties of aromatic amine dehydrogenase from *Pseudomonas* sp., *Arch. Biochem. Biophys. 220*, 253−262.
20. Hothi, P., Khadra, K. A., Combe, J. P., Leys, D., and Scrutton, N. S. (2005) Tryptophan tryptophylquinone cofactor biogenesis in the aromatic amine dehydrogenase of *Alcaligenes faecalis*. Cofactor assembly and catalytic properties of recombinant enzyme expressed in *Paracoccus denitrificans*, *FEBS J. 272*, 5894−5909.
21. Strickland, S., Palmer, G., and Massey, V. (1975) Determination of dissociation constants and specific rate constants of enzyme-substrate (or protein-ligand) interactions from rapid reaction kinetic data, *J. Biol. Chem. 250*, 4048−4052.
22. Otwinowski, Z., and Minor, W. (1997) Processing of X-ray diffraction data collected in oscillation mode, *Methods Enzymol. 276*, 307−326.
23. Murshudov, G. N., Vagin, A. A., and Dodson, E. J. (1997) Refinement of macromolecular structures by the maximum-likelihood method, *Acta Crystallogr. D53*, 240−255.
24. Pudney, C., Hay, S., Sutcliffe, M. J., and Scrutton, N. S. (2006) α-Secondary isotope effects as probes of "tunneling-ready" configurations in enzymatic H-tunneling: Insight from environmentally coupled tunneling models, *J. Am. Chem. Soc. 128*, 14053−14058.
25. Hansch, C., and Leo, A. (1979) *Correlation Analysis in Chemistry and Biology*, Wiley-Interscience, New York.
26. Charton, M. (1969) Nature of the ortho effect. II. Composition of the Taft steric parameters, *J. Am. Chem. Soc. 91*, 615−618.
27. Kutter, E., and Hansch, C. (1969) Steric parameters in drug design. Monoamine oxidase inhibitors and antihistamines, *J. Med. Chem. 12*, 647−652.
28. Idoux, J. P., Hwang, P. T. R., and Hancock, C. K. (1973) Alkaline hydrolysis and nuclear magnetic resonance spectra of some thiol esters, *J. Org. Chem. 38*, 4239−4243.


BI7007239